

Simulating Magnetohydrodynamic Instabilities with Conservative Perturbed MHD Model Using Discontinuous Galerkin Method

Jun Ma^{1,2,*}, Wenfeng Guo^{1,2,*} and Zhi Yu^{1,2}

¹ *Institute of Plasma Physics, Chinese Academy of sciences, Hefei 230031, China.*

² *Center for Magnetic Fusion Theory, Chinese Academy of Sciences, Hefei 230031, China.*

Received 23 June 2016; Accepted (in revised version) 14 October 2016

Abstract. In magnetically confined plasma research, the understandings of small and large perturbations at equilibrium are both critical for plasma controlling and steady state operation. Numerical simulations using original MHD model can hardly give clear picture for small perturbations, while non-conservative perturbed MHD model may break conservation law, and give unphysical results when perturbations grow large after long-time computation. In this paper, we present a nonlinear conservative perturbed MHD model by splitting primary variables in original MHD equations into equilibrium part and perturbed part, and apply an approach in the framework of discontinuous Galerkin (DG) spatial discretization for numerical solutions. This enables high resolution of very small perturbations, and also gives satisfactory non-smooth solutions for large perturbations, which are both broadly concerned in magnetically confined plasma research. Numerical examples demonstrate satisfactory performance of the proposed model clearly. For small perturbations, the results have higher resolution comparing with the original MHD model; for large perturbations, the non-smooth solutions match well with existing references, confirming reliability of the model for instability investigations in magnetically confined plasma numerical research.

AMS subject classifications: 65M60, 65Z05, 85-08

Key words: Discontinuous Galerkin method, conservative perturbed MHD model.

1 Introduction

Numerical simulation of magnetohydrodynamics (MHD) system is always an important subject in magnetically confined plasma research. One of the critical challenging issues of

*Corresponding author. *Email addresses:* junma@ipp.ac.cn (J. Ma), wfguo@ipp.ac.cn (W. Guo), yuzhi@ipp.ac.cn (Z. Yu)

simulating laboratory plasma system is the macroscopic instability analysis in complex geometry, e.g. tokamak and stellarator. In principle, the target of the tokamak or stellarator, aiming for reactor, is to operate the plasma under control as a quasi-steady state system, i.e. equilibrium with perturbations. Large perturbations may lead to confinement degradation or even disruptions. On the other hand, small perturbations are universal and many of them can grow up to large perturbations in long-time operation. Thus the understandings of small and large perturbations are both critical for plasma controlling and maintaining steady state operation. The perturbations are usually of scale comparable with the experimental devices and such macroscopic dynamics of the magnetically confined plasma system can be described by MHD models. Up to now extensive investigations using MHD models have been carried out both analytically and numerically. However for very small perturbations in numerical simulations, the numerical errors generated from the equilibrium part may overwhelm the small perturbations if solving original MHD equations directly. Among fusion community, a widely used way is to split variables in original MHD equations into equilibrium part and perturbed part, resulting in non-conservative compact form MHD equations of perturbations, eliminating numerical errors from equilibrium. Existing simulation codes, such as NIMROD [1] and CLT [2], applying this non-conservative perturbed MHD model, together with classical finite difference methods and finite elements methods, can give good results when solving some instability problems in small perturbations stage, like KH instability and tearing modes. However when small perturbations grow up into strong nonlinear regime, this non-conservative model may lead to unphysical numerical results that break the conservation laws after long time computation, or even end up with numerical disruption, limiting its applications considerably. Although much progress in nonlinear MHD physics in toroidal geometry with these non-conservative MHD model has been made [1, 3], strong nonlinear physics such as disruption [4] are still far from clear and much more efforts are required. So the development of numerical tools for simulating MHD instabilities with high accuracy, robustness and geometrical flexibility is still a hot point in magnetically confined plasma research.

So far many numerical methods and codes for solving conservative MHD models in different geometries have been developed. The most widely used numerical methodologies are based on either finite difference or finite volume spatial discretization. The advanced high order finite difference methods like ENO [5] and WENO [6] type schemes are extensively considered to be simple, effective and easy for code developing, especially on a Cartesian mesh or a mesh that can be mapped onto a Cartesian mesh smoothly. However, due to non-rectangular cross-section of tokamak or stellarator, it is difficult to be applied on such complex geometry. The finite volume method can in general handle the geometry by dividing such space into unstructured meshes, but it is rather complicated to build up high order accuracy schemes [7, 8] on complex stencils. The recently developed numerical framework of discontinuous Galerkin (DG) method is well designed by many authors [9–14]. It is in principle able to achieve arbitrary high order of accuracy on both structured and unstructured mesh and more geometrical flexibility can be acquired.

The stencil of high order schemes under DG framework is also compact and only information of adjacent elements are required. Moreover DG framework is genuinely explicit for temporal discretization so the coding work and parallelization is not difficult. In the past one or two decades DG method has been widely used in different areas including magnetohydrodynamics, turbulent flows, et al., and is becoming more popular [15]. The outstanding advantages of geometrical adaptiveness and high accuracy of DG method make its application to magnetic confinement researches very promising.

As a first step of our long-term MHD simulation in toroidal geometry under DG framework, in the present study, we numerically solve the perturbed MHD equations in conservative form using DG spatial discretization in 2D triangular mesh. This model enables us to investigate the small fluctuations accurately and maintain the advantage of computational robustness, shock capturing ability and reliability in nonlinear regime at the same time, making investigation of instabilities from small amplitude to large amplitude coherently. To control magnetic divergence error and maintain computation stability the hyperbolic divergence cleaning [16, 17] (HDC) correction is applied. It is worthwhile to point out that our approach in principle can be extended to toroidal geometry without essential obstacles.

This paper is organized as follows. In Section 2, we derive the perturbed MHD equations in conservative form. The numerical approach is explained in Section 3. In Section 4, we show several numerical results including both smooth and non-smooth MHD problems, using original and perturbed MHD models respectively. Finally we draw a conclusion.

2 The conservative MHD model for perturbations

We start from the general form of conservation laws as following

$$\partial_t U + \nabla \cdot \vec{F} = 0, \quad (2.1)$$

in which U is conserved variables that can be a scalar or vector, \vec{F} is flux. For conventional ideal or resistive MHD equations, conserved variables are density ρ , momentum $\rho \vec{V}$ where $\vec{V} = u_x \vec{e}_x + u_y \vec{e}_y + u_z \vec{e}_z$ is speed vector with component u_x, u_y, u_z along x, y, z direction respectively. magnetic field $\vec{B} = B_x \vec{e}_x + B_y \vec{e}_y + B_z \vec{e}_z$ and energy $e = \frac{p}{\gamma-1} + \frac{1}{2} \rho V^2 + \frac{1}{2} B^2$ in which adiabatic constant γ is usually set to 5/3. While written in conservation laws as Eq. (2.1) the specific conserved variable vector of MHD is $U = (\rho, \rho u_x, \rho u_y, \rho u_z, e, B_x, B_y, B_z)^T$. The conservative normalized resistive MHD equations can be written as

$$\partial_t \rho + \nabla \cdot (\rho \vec{V}) = 0, \quad (2.2a)$$

$$\partial_t (\rho \vec{V}) + \nabla \cdot \left[\rho \vec{V} \vec{V} - \vec{B} \vec{B} + \left(p + \frac{1}{2} B^2 \right) \vec{I} \right] = 0, \quad (2.2b)$$

$$\partial_t \left(\frac{p}{\gamma-1} + \frac{1}{2} \rho V^2 + \frac{1}{2} B^2 \right) + \nabla \cdot \left[\left(\frac{\gamma p}{\gamma-1} + \frac{1}{2} \rho V^2 + B^2 \right) \vec{V} - (\vec{B} \cdot \vec{V}) \vec{B} + \eta \vec{J} \times \vec{B} \right] = 0, \quad (2.2c)$$

$$\partial_t \vec{B} + \nabla \cdot (\vec{V} \vec{B} - \vec{B} \vec{V} - \eta \nabla \vec{B}) = 0, \quad (2.2d)$$

with a constant resistivity and an additional divergence free constraint $\nabla \cdot \vec{B} = 0$. The equations will reduce to ideal MHD when resistivity is zero.

With the conservative property and numerical approach for hyperbolic conservation laws, these above equations gain success in simulating strong nonlinear problems as magnetic reconnection in space, shock-cloud interaction etc. For magnetically confined plasma system, despite importance of nonlinearity, people are also concerned about small perturbations which may drive instabilities and grow large. However, when using the original MHD to simulate instabilities directly, we will add up equilibrium and small perturbations for initialization. Since the numerical errors are correlated with total amplitude of variables, the concerned perturbed part may be overwhelmed and the structures of such small perturbations cannot be correctly revealed. For perturbed MHD model, numerical errors are only correlated with perturbations, enabling high resolution for small perturbations. But it does suffer disadvantages for non-conservative form. So it is desirable to derive a new perturbed MHD model in conservative form, which can heritage the high resolution property in small perturbation stage, and keep better reliability and robustness in strong nonlinear stage.

In order to derive the perturbed equations, we split all variables into equilibrium part and perturbed part. The equilibrium part (with subscript 0) do not vary with time and their consistency is guaranteed by external analytical or numerical database, i.e. ρ_0 , p_0 , \vec{V}_0 and \vec{B}_0 , while the perturbed part (with tilde above) is time-dependent i.e. $\tilde{U} = U - U_0$, $\tilde{F} = \vec{F} - \vec{F}_0$. The conservative perturbed MHD equations in general form can be written as:

$$\partial_t \tilde{U} + \nabla \cdot \tilde{F} = 0, \quad (2.3)$$

The perturbed conserved variables for ideal MHD equations are:

$$\left\{ \begin{array}{l} \tilde{U}_1 = \tilde{\rho}, \\ \tilde{U}_2 = u_{x0} \tilde{\rho} + \rho_0 \tilde{u}_x + \tilde{\rho} \tilde{u}_x, \\ \tilde{U}_3 = u_{y0} \tilde{\rho} + \rho_0 \tilde{u}_y + \tilde{\rho} \tilde{u}_y, \\ \tilde{U}_4 = u_{z0} \tilde{\rho} + \rho_0 \tilde{u}_z + \tilde{\rho} \tilde{u}_z, \\ \tilde{U}_5 = \frac{\tilde{p}}{\gamma-1} + \frac{1}{2} V_0^2 \tilde{\rho} + \rho (u_{x0} \tilde{u}_x + u_{y0} \tilde{u}_y + u_{z0} \tilde{u}_z) + \frac{1}{2} \rho (\tilde{u}_x^2 + \tilde{u}_y^2 + \tilde{u}_z^2) \\ \quad + (B_{x0} \tilde{B}_x + B_{y0} \tilde{B}_y + B_{z0} \tilde{B}_z) + \frac{1}{2} (\tilde{B}_x^2 + \tilde{B}_y^2 + \tilde{B}_z^2), \\ \tilde{U}_6 = \tilde{B}_x, \\ \tilde{U}_7 = \tilde{B}_y, \\ \tilde{U}_8 = \tilde{B}_z. \end{array} \right. \quad (2.4)$$

The perturbed flux components along x , y , z directions corresponding to each conserved variable are:

$$\left\{ \begin{array}{l} \tilde{F}_{x,1} = u_{x0}\tilde{\rho} + \rho_0\tilde{u}_x + \tilde{\rho}\tilde{u}_x, \\ \tilde{F}_{x,2} = \tilde{p} + \tilde{\rho}u_{x0}^2 + \rho_0\tilde{u}_x(\tilde{u}_x + 2u_{x0}) + (B_{y0}\tilde{B}_y + B_{z0}\tilde{B}_z - B_{x0}\tilde{B}_x) + \frac{1}{2}(\tilde{B}_y^2 + \tilde{B}_z^2 - \tilde{B}_x^2), \\ \tilde{F}_{x,3} = \rho_0u_{x0}\tilde{u}_y + \rho_0\tilde{u}_xu_{y0} + \tilde{\rho}u_{x0}u_{y0} + \rho_0\tilde{u}_x\tilde{u}_y + \tilde{\rho}u_{x0}\tilde{u}_y + \tilde{\rho}\tilde{u}_xu_{y0} + \tilde{\rho}\tilde{u}_x\tilde{u}_y \\ \quad - (B_{x0}\tilde{B}_y + \tilde{B}_xB_{y0} + \tilde{B}_x\tilde{B}_y), \\ \tilde{F}_{x,4} = \rho_0u_{x0}\tilde{u}_z + \rho_0\tilde{u}_xu_{z0} + \tilde{\rho}u_{x0}u_{z0} + \rho_0\tilde{u}_x\tilde{u}_z + \tilde{\rho}u_{x0}\tilde{u}_z + \tilde{\rho}\tilde{u}_xu_{z0} + \tilde{\rho}\tilde{u}_x\tilde{u}_z \\ \quad - (B_{x0}\tilde{B}_z + \tilde{B}_xB_{z0} + \tilde{B}_x\tilde{B}_z), \\ \tilde{F}_{x,5} = \tilde{u}_xH_0 + u_{x0}\tilde{H} + \tilde{u}_x\tilde{H} - \tilde{B}_x\mu_0 - B_{x0}\tilde{\mu} - \tilde{B}_x\tilde{\mu}, \\ \tilde{F}_{x,6} = 0, \\ \tilde{F}_{x,7} = B_{y0}\tilde{u}_x + \tilde{B}_yu_{x0} - B_{x0}\tilde{u}_y - \tilde{B}_xu_{y0} + \tilde{B}_y\tilde{u}_x - \tilde{B}_x\tilde{u}_y, \\ \tilde{F}_{x,8} = B_{z0}\tilde{u}_x + \tilde{B}_zu_{x0} - B_{x0}\tilde{u}_z - \tilde{B}_xu_{z0} + \tilde{B}_z\tilde{u}_x - \tilde{B}_x\tilde{u}_z, \end{array} \right. \quad (2.5a)$$

$$\left\{ \begin{array}{l} \tilde{F}_{y,1} = u_{y0}\tilde{\rho} + \rho_0\tilde{u}_y + \tilde{\rho}\tilde{u}_y, \\ \tilde{F}_{y,2} = \rho_0u_{x0}\tilde{u}_y + \rho_0\tilde{u}_xu_{y0} + \tilde{\rho}u_{x0}u_{y0} + \rho_0\tilde{u}_x\tilde{u}_y + \tilde{\rho}u_{x0}\tilde{u}_y + \tilde{\rho}\tilde{u}_xu_{y0} + \tilde{\rho}\tilde{u}_x\tilde{u}_y \\ \quad - (B_{x0}\tilde{B}_y + \tilde{B}_xB_{y0} + \tilde{B}_x\tilde{B}_y), \\ \tilde{F}_{y,3} = \tilde{p} + \tilde{\rho}u_{y0}^2 + \rho_0\tilde{u}_y(\tilde{u}_y + 2u_{y0}) + (B_{x0}\tilde{B}_x + B_{z0}\tilde{B}_z - B_{y0}\tilde{B}_y) + \frac{1}{2}(\tilde{B}_x^2 + \tilde{B}_z^2 - \tilde{B}_y^2), \\ \tilde{F}_{y,4} = \rho_0u_{y0}\tilde{u}_z + \rho_0\tilde{u}_yu_{z0} + \tilde{\rho}u_{y0}u_{z0} + \rho_0\tilde{u}_y\tilde{u}_z + \tilde{\rho}u_{y0}\tilde{u}_z + \tilde{\rho}\tilde{u}_yu_{z0} + \tilde{\rho}\tilde{u}_y\tilde{u}_z \\ \quad - (B_{y0}\tilde{B}_z + \tilde{B}_yB_{z0} + \tilde{B}_y\tilde{B}_z), \\ \tilde{F}_{y,5} = \tilde{u}_yH_0 + u_{y0}\tilde{H} + \tilde{u}_y\tilde{H} - \tilde{B}_y\mu_0 - B_{y0}\tilde{\mu} - \tilde{B}_y\tilde{\mu}, \\ \tilde{F}_{y,6} = B_{x0}\tilde{u}_y + \tilde{B}_xu_{y0} - B_{y0}\tilde{u}_x - \tilde{B}_yu_{x0} + \tilde{B}_x\tilde{u}_y - \tilde{B}_y\tilde{u}_x, \\ \tilde{F}_{y,7} = 0, \\ \tilde{F}_{y,8} = B_{z0}\tilde{u}_y + \tilde{B}_zu_{y0} - B_{y0}\tilde{u}_z - \tilde{B}_yu_{z0} + \tilde{B}_z\tilde{u}_y - \tilde{B}_y\tilde{u}_z, \end{array} \right. \quad (2.5b)$$

$$\left\{ \begin{array}{l} \tilde{F}_{z,1} = u_{z0}\tilde{\rho} + \rho_0\tilde{u}_z + \tilde{\rho}\tilde{u}_z, \\ \tilde{F}_{z,2} = \rho_0u_0\tilde{u}_z + \rho_0\tilde{u}_xu_{z0} + \tilde{\rho}u_{x0}u_{z0} + \rho_0\tilde{u}_x\tilde{u}_z + \tilde{\rho}u_{x0}\tilde{u}_z + \tilde{\rho}\tilde{u}_xu_{z0} + \tilde{\rho}\tilde{u}_x\tilde{u}_z \\ \quad - (B_{x0}\tilde{B}_z + \tilde{B}_xB_{z0} + \tilde{B}_x\tilde{B}_z), \\ \tilde{F}_{z,3} = \rho_0u_{y0}\tilde{u}_z + \rho_0\tilde{u}_yu_{z0} + \tilde{\rho}u_{y0}u_{z0} + \rho_0\tilde{u}_y\tilde{u}_z + \tilde{\rho}u_{y0}\tilde{u}_z + \tilde{\rho}\tilde{u}_yu_{z0} + \tilde{\rho}\tilde{u}_y\tilde{u}_z \\ \quad - (B_{y0}\tilde{B}_z + \tilde{B}_yB_{z0} + \tilde{B}_y\tilde{B}_z), \\ \tilde{F}_{z,4} = \tilde{p} + \tilde{\rho}u_{z0}^2 + \rho_0\tilde{u}_z(\tilde{u}_z + 2u_{z0}) + (B_{x0}\tilde{B}_x + B_{y0}\tilde{B}_y - B_{z0}\tilde{B}_z) + \frac{1}{2}(\tilde{B}_x^2 + \tilde{B}_y^2 - \tilde{B}_z^2), \\ \tilde{F}_{z,5} = \tilde{u}_zH_0 + u_{z0}\tilde{H} + \tilde{u}_z\tilde{H} - \tilde{B}_z\mu_0 - B_{z0}\tilde{\mu} - \tilde{B}_z\tilde{\mu}, \\ \tilde{F}_{z,6} = B_{x0}\tilde{u}_z + \tilde{B}_xu_{z0} - B_{z0}\tilde{u}_x - \tilde{B}_zu_{x0} + \tilde{B}_x\tilde{u}_z - \tilde{B}_z\tilde{u}_x, \\ \tilde{F}_{z,7} = B_{y0}\tilde{u}_z + \tilde{B}_yu_{z0} + \tilde{B}_y\tilde{u}_z - B_{z0}\tilde{u}_y - \tilde{B}_zu_{y0} - \tilde{B}_z\tilde{u}_y, \\ \tilde{F}_{z,8} = 0, \end{array} \right. \quad (2.5c)$$

in which $H = \frac{\gamma p}{\gamma - 1} + \frac{1}{2}\rho V^2 + B^2$ is enthalpy and $\mu = \vec{B} \cdot \vec{V}$ is magnetic momentum. With consistent equilibrium data this perturbed model is analytically equivalent to the original MHD equations (2.2) while numerically different. No approximation is made when deriving this model. So it is still nonlinear and there are no limitations for parameters. In the following, we use subscript PER and ORG to represent this new perturbed MHD model and original MHD model, respectively. Notice if all equilibrium parameters are set to zero, the MHD_{PER} system will be equivalent to the conventional MHD_{ORG} model.

3 Numerical approach

Discontinuous Galerkin method combines the spatial discretization techniques in finite volume and finite element method. In this method a space of polynomial basis and test functions in specific element is used, and weak form of hyperbolic conservation laws is applied. Numerical flux on element interfaces are required through a similar way as in a finite volume method, and advantages of such numerical scheme with high accuracy, geometrical flexibility and upwind properties remain for convection dominated problems. In this section, we briefly describe our numerical approach based on the framework of Runge-Kutta discontinuous Galerkin (RKDG) method [9–14].

3.1 Spatial discretization by discontinuous Galerkin method

We explain this numerical method on a two dimension computation domain Ω , which is to be divided into nonoverlapping triangles. Given an element K of the triangulation T_h of Ω , a finite dimensional polynomial space $U(K)$ can be defined. If one has an approximate solution $u_h(\vec{x}) \in U(K)$ in the element, $u_h(\vec{x}) = \sum_{i=1}^{N_p} u_i \phi_i(\vec{x})$ and $\phi_i(\vec{x})$ are any of N_p polynomial bases with highest order k chosen from the polynomial space so $N_p = \frac{(k+1)(k+2)}{2}$, u_i are coefficients. Notice here $u_h(\vec{x})$ can be discontinuous over adjacent elements.

For any test function $v_h(\vec{x}) \in U(K)$, multiply v_h with the conservation law and integrate over element K , one obtains

$$\int_K \partial_t u_h \cdot v_h d\vec{x} = \int_K \vec{f} \cdot \nabla v_h d\vec{x} - \int_{\partial K} (\hat{f} \cdot \vec{n}) v_h ds, \quad (3.1)$$

where \vec{n} is interface norm vector of boundary ∂K pointing towards outside and \hat{f} is corresponding numerical flux. In practical applications v_h is often selected from one of those N_p polynomial bases $\{\phi_i(\vec{x})\}$, resulting subsequent equations from Eq. (3.1). To solve the discretized equations in an easier form and with better efficiency, we choose a set of k -th order orthonormal polynomial bases $\{\varphi_i(\vec{x})\}$ on the standard triangle K_0 composed of points (0,0)-(1,0)-(0,1) on two dimensional plane that

$$\int_{K_0} \varphi_i(\vec{x}) \varphi_j(\vec{x}) d\vec{x} = \delta_{ij}, \quad i, j = 1, 2, \dots, N_p.$$

Then for each triangle element K the polynomial bases $\{\phi_i(\vec{x})\}$ is linearly mapped from $\{\varphi_i(\vec{x})\}$ on K_0 and

$$\int_K \phi_i(\vec{x})\phi_j(\vec{x})d\vec{x} = 2S_K\delta_{ij}, \quad i, j = 1, 2, \dots, N_p,$$

where S_K is area of element K . Eq. (3.1) then can be rewritten as:

$$\frac{du_i}{dt} = \frac{1}{2S_K} \int_K \vec{f} \cdot \nabla \phi_i d\vec{x} - \frac{1}{2S_K} \int_{\partial K} (\hat{f} \cdot \vec{n}) \phi_i ds. \quad (3.2)$$

The first term on the right hand side of Eq. (3.2) can be numerically computed through Gauss quadrature formulations on triangles or other quadrature-free procedure with accuracy up to order $2k$, while the second term should also be obtained through Gauss-Legendre quadrature procedure on each side of triangle K with accuracy up to order $2k+1$. In the second term, numerical flux on element interfaces could be obtained by solving a Riemann problem accurately or approximately in a similar way as in finite volume method:

$$(\hat{f} \cdot \vec{n})_{\partial K} = (\hat{f} \cdot \vec{n})(u_{h,\partial K}^-, u_{h,\partial K}^+),$$

which means the numerical flux should be determine by discontinuous u_h value on both sides of the element interface, where the superscript $+$ indicates the outer side and $-$ indicates the inner side. A simple and straightforward choice is the local Lax-Friedrichs flux:

$$(\hat{f} \cdot \vec{n})^{LF}(a, b) = \frac{1}{2} [f(a) + f(b)] \cdot \vec{n} - \frac{C}{2} (b - a), \quad (3.3)$$

where $C = \max(C_a, C_b)$ is maximum absolute local characteristic speed on both sides. For MHD system,

$$C_j = |\vec{V}_j \cdot \vec{n}| + \sqrt{\frac{\gamma p_j + B_j^2 + \sqrt{(\gamma p_j + B_j^2)^2 - 4\gamma p_j (\vec{B}_j \cdot \vec{n})^2}}{2\rho_j}}, \quad j = a, b. \quad (3.4)$$

And the interface norm vector points from a side to b side.

For MHD_{ORG} and MHD_{PER} models illustrated before, they have formally the same numerical schemes. The expressions of perturbed conserved variables and fluxes on quadrature points of the triangle can be found in Eq. (2.4) and Eq. (2.5). For numerical flux on element boundary, both MHD_{PER} and MHD_{ORG} model use the same parameter C as defined in Eq. (3.4). In the MHD_{PER} model, equilibrium data on Gauss quadrature points of elements and interfaces are required before computation.

3.2 Constraint of free magnetic divergence

Another major challenge in using DG discretization for solving our MHD system is the divergence free constraint $\nabla \cdot \vec{B} = 0$. Although a divergence free initial condition guaranteed zero divergence by model Eq. (2.2d), in numerical calculation the divergence error

is inevitable, which will accumulate in time, and pollute the solution or even destroy the computation [18]. In the frame work of DG, many recent works have overcome this difficulty by using exactly divergence-free [19–21] or locally divergence-free [22,23] techniques. These indeed gave satisfactory results.

In the present work, we apply the hyperbolic divergence cleaning (HDC) method proposed by Dedner [16], which has also been applied for MHD simulation in the framework of DG method successfully [17]. Since the MHD_{PER} model is equivalent to MHD_{ORG} model if setting equilibrium to zero, we only illustrate its application in the MHD_{PER} model. The equilibrium magnetic field satisfies $\nabla \cdot \vec{B}_0 = 0$, so in the MHD_{PER} model we only need to consider the divergence free constraint upon $\nabla \cdot \vec{B} = 0$. By introducing a new auxiliary variable, the general Lagrange multiplier (GLM) ψ as the ninth variable, we add an additional equation

$$\partial_t \psi + c_h^2 \nabla \cdot \vec{B} = -\frac{c_h^2}{c_p^2} \psi, \quad (3.5)$$

to MHD system. c_h and c_p are constants. As in Ref. [16], c_h is estimated from the global maximum characteristic speed and c_p is empirically set to $c_p^2 = 0.18c_h$. Then the magnetic field conservation equation is modified to

$$\partial_t \vec{B} + \nabla \cdot (\vec{V} \vec{B}_0 + \vec{V}_0 \vec{B} + \vec{V} \vec{B} - \vec{B} \vec{V}_0 - \vec{B}_0 \vec{V} - \vec{B} \vec{V}) = 0. \quad (3.6)$$

In this modified system, the numerically generated divergence errors will be transported to the domain boundaries with certain speed and damped at the same time. For our numerical scheme, to apply this HDC technique, only very simple modification is needed. More specifically, according to Eq. (3.6) the corresponding flux terms of Eq. (2.5a) to Eq. (2.5c) would be slightly modified as

$$\tilde{F}_{x,6} = \tilde{F}_{y,7} = \tilde{F}_{z,8} = \psi, \quad (3.7)$$

And the fluxes of Eq. (3.5) are as following

$$\begin{cases} \tilde{F}_{x,9} = c_h^2 \tilde{B}_x, \\ \tilde{F}_{y,9} = c_h^2 \tilde{B}_y, \\ \tilde{F}_{z,9} = c_h^2 \tilde{B}_z. \end{cases} \quad (3.8)$$

For boundary fluxes through element interfaces the sixth and newly added ninth numerical flux component will be given as

$$\begin{cases} (\tilde{F} \cdot \vec{n})_6 = \frac{\psi^+ + \psi^-}{2} - \frac{c_h}{2} (\tilde{B}_n^+ - \tilde{B}_n^-), \\ (\tilde{F} \cdot \vec{n})_9 = \frac{c_h^2}{2} (\tilde{B}_n^+ + \tilde{B}_n^-) - \frac{c_h}{2} (\psi^+ - \psi^-). \end{cases} \quad (3.9)$$

Here subscript n means vector component along \vec{n} direction. The source term on the right hand side of Eq. (3.5) will be discussed in time discretization subsection. These modifications of existing numerical scheme are rather simple. Moreover, this idea can easily be extended to arbitrary high order schemes and any kind of meshes.

3.3 Nonlinear limiter

For the stability of computation in nonlinear non-smooth problems, nonlinear limiters are needed. The generalized total variation bounded minmod (TVBM) slope limiter with a constant M from [13,14] for triangular mesh is applied in our present work in component-wise fashion.

3.4 Time discretization

The DG spatial discretization with application of HDC technique above leads to the method of line ODE system:

$$\frac{du}{dt} = L(u), \quad (3.10)$$

Where u stands for time evolving coefficients. This semi-discretized equations can be further discretized by using strong stability preserving (SSP) methods [24,25] as illustrated below:

$$\begin{cases} u^{(1)} = u^n + \Delta t_n L(u^n), \\ u^{(2)} = \frac{3}{4}u^n + \frac{1}{4}u^{(1)} + \frac{1}{4}\Delta t_n L(u^{(1)}), \\ u^{n+1} = \frac{1}{3}u^n + \frac{2}{3}u^{(2)} + \frac{2}{3}\Delta t_n L(u^{(2)}). \end{cases} \quad (3.11)$$

Superscript n and $n+1$ stand for numerical solution at t_n and t_{n+1} with time step $\Delta t_n = t_{n+1} - t_n$. After each component of the system is advanced by Runge-Kutta time integration, the general Lagrange multiplier should be rescaled by a factor $e^{-\Delta t \cdot c_h^2 / c_p^2}$ due to HDC method. This completes our numerical approach.

4 Simulation results

In this section, we report a series of numerical experiments including accuracy tests, non-linear Kelvin-Helmholtz instability and coalescence instability with small perturbations and large perturbations, Orszag-Tang vortex problem in a slightly different way. All tests are carried out on two dimensional triangular meshes. Rectangular simulation domain is first divided into Cartesian mesh and then each small rectangle is divided into two equal triangles. The order of accuracy ranges from two to four, i.e. $k=1,2,3$.

4.1 Accuracy tests

It is necessary to perform accuracy tests before we test other numerical examples. Smooth Alfvén wave problem and Smooth vortex problem are tested with $k=1,2,3$. In this subsection we use the MHD_{ORG} model for accuracy tests, i.e. all equilibrium parameters are set to zero.

4.1.1 Smooth Alfvén wave

This case describes a circularly polarized Alfvén wave [21,23] propagating at a constant speed in the domain $[0,1/\cos\alpha] \times [0,1/\sin\alpha]$ with initial condition as follows:

$$\rho=1, u_{\parallel}=0, u_{\perp}=0.1\sin(2\pi\beta), u_z=0.1\cos(2\pi\beta), B_{\parallel}=1, B_{\perp}=u_{\perp}, B_z=u_z, p=0.1,$$

and periodic boundary condition. $\alpha = \pi/4$ is the angle of x -axis and wave-propagating direction, $\beta = x\cos\alpha + y\sin\alpha$, and subscripts \parallel stands for direction parallel to the wave propagation direction while \perp for perpendicular. With the constant Alfvén wave speed ($B_{\parallel}/\sqrt{\rho}=1$) and the size of the periodic domain, all variables return to initial state once time variable t is added by unity. L_2 errors and orders of ρ , u_x , p and B_x at $t=5$ are obtained for $k=1,2,3$ in Table 1. In general satisfactory accuracy is achieved.

Table 1: Smooth Alfvén wave problem, L_2 errors and orders for $t=5$.

N	ρ		u_x		p		B_x	
	L_2 error	order	L_2 error	order	L_2 error	order	L_2 error	order
$k=1$								
16	6.61e-4	—	5.00e-3	—	1.08e-3	—	5.00e-3	—
32	1.77e-4	1.90	6.80e-4	2.88	1.69e-4	2.67	6.91e-4	2.86
64	4.44e-5	1.99	8.97e-5	2.92	3.03e-5	2.49	9.63e-5	2.84
128	1.11e-5	2.00	1.28e-5	2.80	6.55e-6	2.21	1.56e-5	2.63
$k=2$								
16	2.29e-3	—	6.54e-5	—	3.12e-5	—	4.96e-5	—
32	1.58e-4	3.86	9.74e-6	2.75	3.04e-6	3.36	6.15e-6	3.01
64	9.95e-6	3.99	1.33e-6	2.87	4.03e-7	2.92	7.80e-7	2.98
128	7.71e-7	3.69	1.68e-7	2.99	7.00e-8	2.52	9.42e-8	3.05
$k=3$								
16	7.73e-5	—	1.99e-6	—	5.59e-6	—	4.40e-6	—
32	5.07e-6	3.93	1.13e-7	4.14	1.49e-7	5.23	1.62e-7	4.76
64	1.10e-7	5.53	7.14e-9	3.98	5.48e-9	4.78	8.72e-9	4.21
128	3.63e-9	4.92	4.69e-10	3.93	2.56e-10	4.42	5.41e-10	4.01

4.1.2 Smooth vortex problem

In this case [26], a vortex with perturbations in velocity and magnetic field is dynamically balanced by pressure, and moves stably with a constant speed vector $(1,1)$. Following is the initial configuration:

$$\rho=1, u_x=1+\delta u_x, u_y=1+\delta u_y, u_z=0, B_x=\delta B_x, B_y=\delta B_y, B_z=0, p=1+\delta p,$$

where

$$\phi = \frac{1}{2\pi} \exp\left(\frac{1-r^2}{2}\right), \quad \delta\vec{u} = \eta \nabla\phi \times \vec{e}_z, \quad \delta\vec{B} = \zeta \nabla\phi \times \vec{e}_z,$$

$$\delta p = \frac{1}{2}[\zeta^2(1-r^2) - \eta^2]\phi^2, \quad r^2 = x^2 + y^2, \quad \zeta = 1, \quad \eta = 1.$$

Periodic boundary condition is applied on domain $[-L, L] \times [-L, L]$, and the vortex goes back to initial state every $t = 2L$. The initial perturbed velocity, magnetic field and pressure reduce to zero toward the boundary, and the domain size L is chosen to make the boundary error to ignorable level. We chose total time in computation for the vortex to recover its initial state twice, so the parameters are $L = 5$, $t = 20$ for $k = 1$, and $L = 10$, $t = 40$ for $k = 2$ and $k = 3$. L_2 errors and orders of ρ , u_x , p and B_x are obtained in Table 2. It is observed that $k = 1$ results are good enough and $k = 2$ results suffer accuracy lost about half an order. The $k = 3$ results seem to lose a little accuracy. The lost in accuracy is also observed in Ref. [23] due to smaller locally divergence-free polynomial space. This accuracy lost is possibly induced by the HDC technique.

Table 2: Smooth vortex problem, L_2 errors and orders.

N	ρ		u_x		p		B_x	
	L_2 error	order	L_2 error	order	L_2 error	order	L_2 error	order
$k=1, L=5, T=20$								
16	3.88e-4	—	9.09e-3	—	1.32e-3	—	1.03e-2	—
32	1.48e-4	1.39	1.92e-3	2.25	3.51e-4	1.91	2.39e-3	2.11
64	3.09e-5	2.26	2.67e-4	2.82	6.31e-5	2.48	3.46e-4	2.79
128	6.77e-6	2.19	3.49e-5	2.94	1.23e-5	2.36	4.53e-5	2.93
$k=2, L=10, T=40$								
16	2.81e-4	—	3.89e-3	—	5.81e-4	—	4.32e-3	—
32	9.09e-5	1.63	5.27e-4	2.88	1.35e-4	2.11	5.95e-4	2.86
64	1.54e-5	2.56	4.88e-5	3.43	2.34e-5	2.53	5.04e-5	3.54
128	2.24e-6	2.78	9.14e-6	2.42	3.56e-6	2.71	9.13e-6	2.47
$k=3, L=10, T=40$								
16	1.70e-4	—	9.59e-4	—	1.87e-4	—	1.06e-3	—
32	1.37e-5	3.63	3.54e-5	4.76	1.06e-5	4.15	3.71e-5	4.84
64	3.19e-7	5.43	1.79e-6	4.30	4.82e-7	4.45	1.79e-6	4.37
128	1.58e-8	4.33	1.27e-7	3.82	2.57e-8	4.23	1.28e-7	3.80

4.2 Instabilities with small perturbations

When numerically investigating linear dynamic of MHD instability at a specific equilibrium configuration by using a time-evolution method, one usually starts from equilibrium with very small perturbations. Comparing with the linear result obtained by linear model, the smaller the perturbation is, the closer the numerical result should be. However in the MHD_{ORG} model, the numerical error is estimated by the total amount of variables, which may overwhelm the small perturbations we are interested in. If we

use the MHD_{PER} model, the small perturbations can avoid being polluted by numerical errors from discretized inhomogeneous equilibrium. In the following tests we compare results given by both the MHD_{ORG} model and the MHD_{PER} model with $k=1,2,3$.

4.2.1 Linear Kelvin-Helmholtz instability

The first experiment is the Kelvin-Helmholtz(KH) instability which occurs at the interface between two fluids or plasmas moving in opposite directions. This model is solved in a two dimensional rectangle with $0 \leq x \leq L_x$ and $-L_y \leq y \leq L_y$, $L_x = L_y = 1$, The equilibrium parameters are given as following [27]:

$$\rho_0 = 1, \quad u_{x0} = V_0 \tanh(y/a), \quad p_0 = 1, \quad B_{x0} = 0.129,$$

where $a=0.05$, $V_0=0.645$, and all other equilibrium parameters are zero. The present perturbation is only $\delta u_y = \varepsilon \sin(k_x x) \exp[-(y/0.2)^2]$, with $k_x = 2\pi/L_x$. ε is assumed to be very small, for instance 1.0×10^{-6} , in order to investigate growth rate Γ of the linear instability, which is evaluated through exponential fitting, $E_y = \iint dx dy (\rho v_y^2) / 2 \sim \exp(2\Gamma t)$, or linear fitting of $\ln E_y$ in linear stage.

We first divide the domain into $N \times (2N)$ small squares, and then split each square into two triangles. Periodic boundary condition is applied in x direction. Lots of simulations have been carried out with different N and accuracy for both models. We show the results in Fig. 1. The dotted line parallel to x axis indicates the results of linear growth rate $\Gamma a/V = 0.1320$ obtained on an $N=100$ refined mesh by both MHD_{PER} and MHD_{ORG} models, as a reference value. The results show that in general the MHD_{PER} model converges faster than the MHD_{ORG} model. For $k=1$, the MHD_{PER} result in satisfactory growth rate at $N=45$, while MHD_{ORG} requires at least $N=70$; For $k=2$ the numbers of discretization are $N=25$ and $N=40$; For $k=3$ they are $N=15$ and $N=35$. The results also show that with same mesh the high order scheme gives more accurate results than lower ones both for MHD_{PER} and MHD_{ORG} models.

Another advantage of MHD_{PER} model is its much better resolution of linear structure as can be seen in Fig. 2. Contour plot of perturbed density with different models clearly demonstrate that the small perturbation is apparently smeared by numerical errors in MHD_{ORG} model. This smearing of small perturbations in MHD_{ORG} model is even more serious with lower order schemes, coarser mesh and earlier stage of the linear phase.

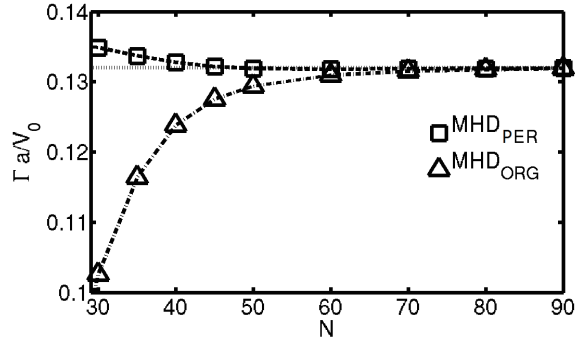
4.2.2 Linear Coalescence instability

This experiment [28] starts near a smooth equilibrium with the following parameters:

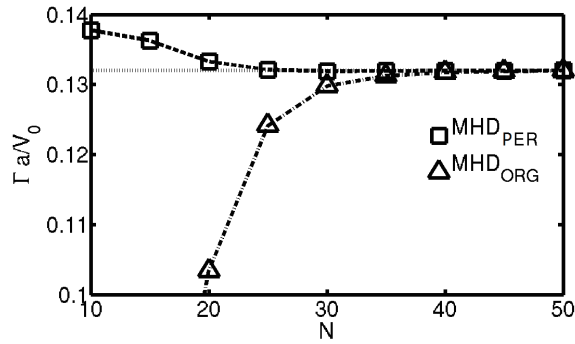
$$\begin{aligned} \rho_0 &= 1, \quad p_0 = 1 + 8\pi^2 A_0^2, \quad B_{x0} = 0.2\pi \sin(4\pi y), \\ B_{y0} &= 0.2\pi \sin(4\pi x), \quad A_0 = 0.05[\cos(4\pi x) - \cos(4\pi y)], \end{aligned}$$

other equilibrium parameters are set to zero. The initial perturbation is only in velocity field:

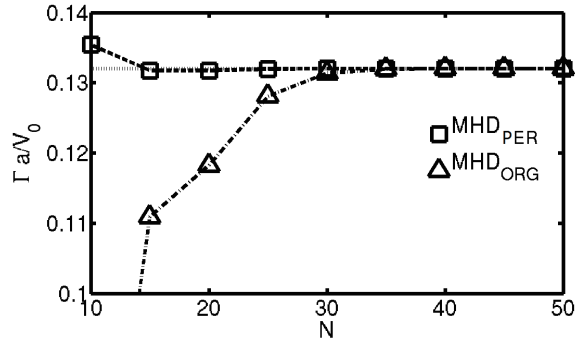
$$\delta u_x = \varepsilon \sin(2\pi x) \cos(2\pi y), \quad \delta u_y = -\varepsilon \sin(2\pi y) \cos(2\pi x),$$



(a)



(b)



(c)

Figure 1: Linear growth rate of KH instability obtained by MHD_{PER} and MHD_{ORG} model with different N . Dotted line indicates a reference value.

with the perturbation amplitude $\varepsilon \ll 1$. The periodic computation domain is $[-0.5, 0.5] \times [-0.5, 0.5]$ and divided into $N \times N \times 2$ triangles.

In this computation we set $\varepsilon = 1 \times 10^{-5}$. Linear growth rate is evaluated through ex-

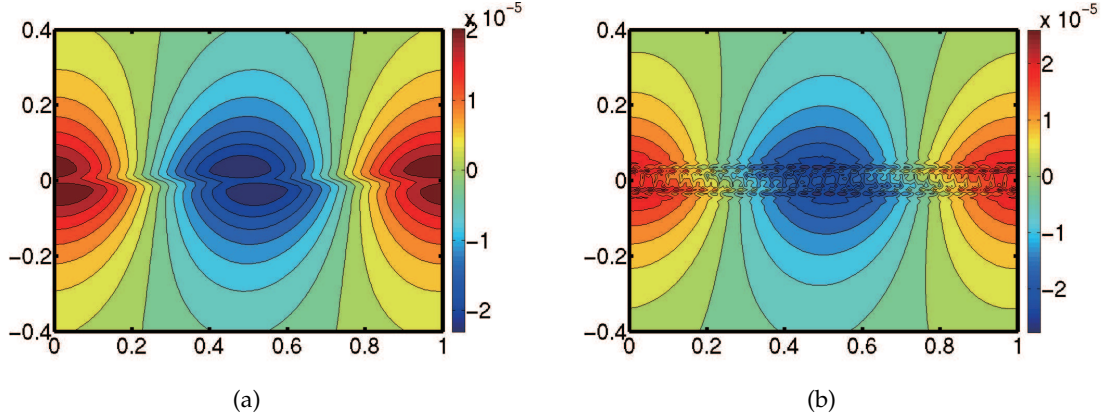


Figure 2: Contour plot of perturbed density at $t=3$ on $N=30$ mesh with $k=3$. (a) MHD_{PER} model; (b) MHD_{ORG} model.

ponential fitting of the kinetic energy $E_K = \iint dx dy (\rho V^2) / 2 \sim \exp(2\Gamma t)$ or linear fitting of $\ln E_K$ in linear stage. A reference value $2\Gamma / \ln 10 = 2.02$ is obtained on an $N=200$ mesh by both MHD_{PER} and MHD_{ORG} models with $k=3$. The results in Fig. 3 show that linear growth rate obtained by the MHD_{PER} model converges faster than the MHD_{ORG} model in general. For $k=1$, the MHD_{ORG} model does not give satisfactory accuracy even at $N=100$; For $k=2$ the MHD_{PER} model converge at $N=50$ and the MHD_{ORG} model at $N=60$; For $k=3$ they are $N=30$ and $N=35$. High order scheme also gives more accurate results than lower ones.

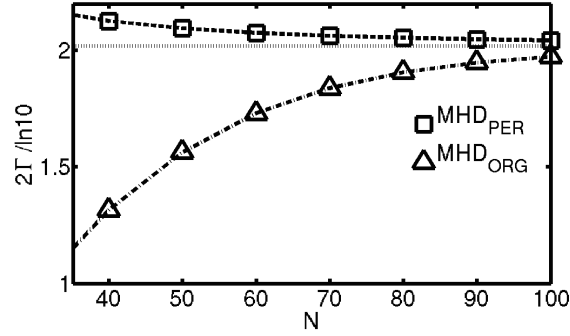
We investigate the structures of perturbed magnetic flux \vec{A} which is defined by $\vec{B} = \nabla A \times \vec{e}_z$, at linear stage using both MHD_{PER} and MHD_{ORG} model. The contour plot of \vec{A} on an $N=20$ mesh with $k=3$ at $t=1.5$ is shown in Fig. 4. The linear structure of perturbed magnetic flux obtained by the MHD_{PER} model on such a coarse mesh matched with the result in Fig. 6 of Ref. [28] rather well, while the result from the MHD_{ORG} model suffers visible smearing.

4.3 Instabilities with large perturbations

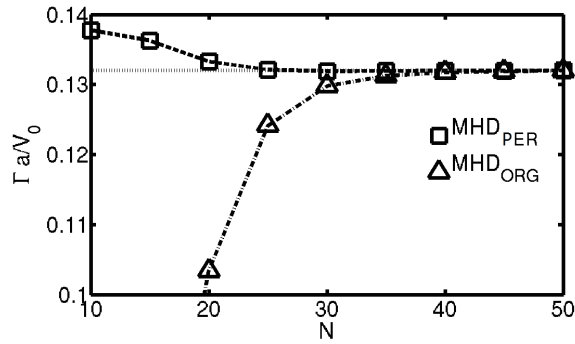
When we use the MHD_{PER} numerical model to investigate nonlinear dynamics, or instabilities grow up from small perturbation to strong nonlinearity, the model should maintain the ability of solving non-smooth problems in strong nonlinearity with the application of the TVBM limiter. Here we show the nonlinear stage of the KH instability and coalescence instability in Section 4.2. Also Orszag-Tang vortex with the presence of a given artificial equilibrium is tested.

4.3.1 Nonlinear KH instability

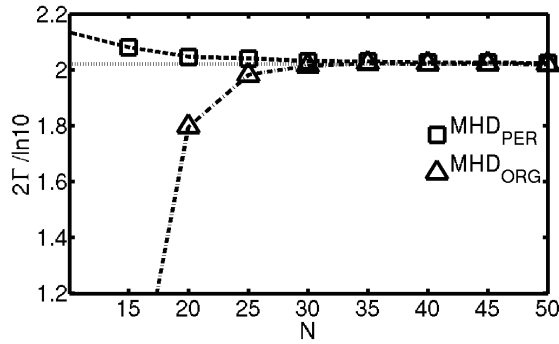
This example is the nonlinear stage of the tested linear KH instability in Section 4.2. When the linear instability further develops, the perturbation will rise up to equilibrium level,



(a)



(b)



(c)

Figure 3: Linear growth rate of Coalescence instability obtained by MHD_{PER} and MHD_{ORG} model with different N . Dotted line indicates a reference value $2\Gamma/\ln 10=2.02$. (a) $k=1$; (b) $k=2$; (c) $k=3$.

leading to non-smooth structures. By applying the MHD_{PER} model we take this computation on an $N=200$ domain with $k=2$ and TVBM parameter $M=10$. To achieve the nonlinear stage earlier, we start with a larger perturbation level $\varepsilon=1 \times 10^{-2}$. The contour

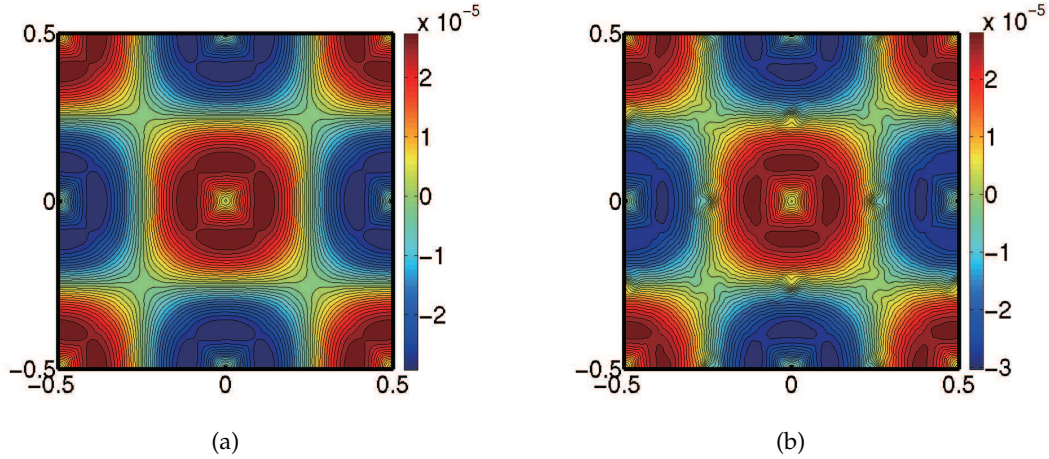


Figure 4: Structure of perturbed magnetic flux of Coalescence instability at $t=1.5$ obtained with $k=3$ scheme on $N=20$ mesh. (a) MHD_{PER} model; (b) MHD_{ORG} model.

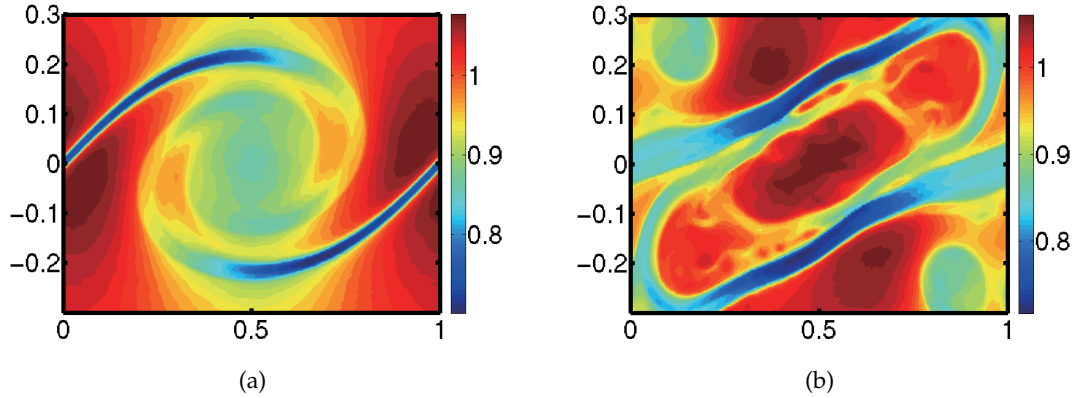


Figure 5: Contour plot of density of KH instability in nonlinear stage. (a) $t=4$; (b) $t=6$. The computation was carried out with MHD_{PER} model on an $N=200$ mesh with $k=2$ scheme, $M=10$.

plot of density within area $[0,1] \times [-0.3,0.3]$ at $t=4$ and $t=6$ are displayed in Fig. 5. The plots are matched well with the Fig. 9 of Ref. [27].

4.3.2 Nonlinear coalescence instability

This example is the nonlinear stage of the linear coalescence instability in Section 4.2. With $N=200$, $k=2$ and $M=10$, we display the total magnetic flux A at $t=4.8$ when the kinetic energy reach the first local maxima. The contour lines in Fig. 6 clearly show the pentagon structure of magnetic field lines in nonlinear stage, which is well matched with Fig. 8 of Ref. [28].

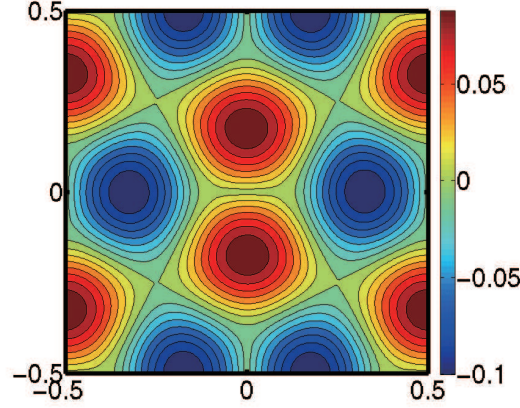


Figure 6: Contour plot of magnetic flux of coalescence instability in nonlinear stage at $t=4.8$. The computation was carried out with MHD_{PER} model on an $N=200$ mesh with $k=2$ scheme, $M=10$.

4.3.3 Orszag-Tang vortex

This is a widely used example in MHD simulations. The computation domain is $[0, 2\pi] \times [0, 2\pi]$ divided into $N \times N \times 2$ triangles with initial conditions:

$$\rho = \gamma^2, \quad u_x = -\sin y, \quad u_y = \sin x, \quad u_z = 0, \quad p = \gamma, \quad B_x = -\sin y, \quad B_y = \sin 2x, \quad B_z = 0.$$

Different from conventional test, we introduce an artificial inhomogeneous smooth equilibrium:

$$\rho_0 = 2, \quad p_0 = 1 + 2A_0^2, \quad B_{x0} = 0.4\sin 2y, \quad B_{y0} = 0.4\sin 2x, \quad A_0 = 0.2(\cos 2x - \cos 2y).$$

With such ‘‘equilibrium’’ we use MHD_{PER} model with $N = 200$, $k = 2$ and $M = 5$ to test the ability of the MHD_{PER} numerical methods. The simulation went on stably and the results are in agreement with others, e.g. [21]. The density contours at different time are displayed in Fig. 7.

5 Concluding remarks

In summary, we present a nonlinear conservative perturbed MHD model, and apply a numerical approach in the framework of DG spatial discretization in 2D triangular mesh. To accommodate the magnetically confined plasma system, we split the variables in original MHD equations into equilibrium part and perturbed part, resulting in conservative form MHD equations of perturbations and eliminating numerical errors from equilibrium. With this model and DG approach, we are able to investigate instabilities from small amplitude to large amplitude coherently with reasonable results. For small perturbations, this conservative perturbed MHD model gives more accurate results in early

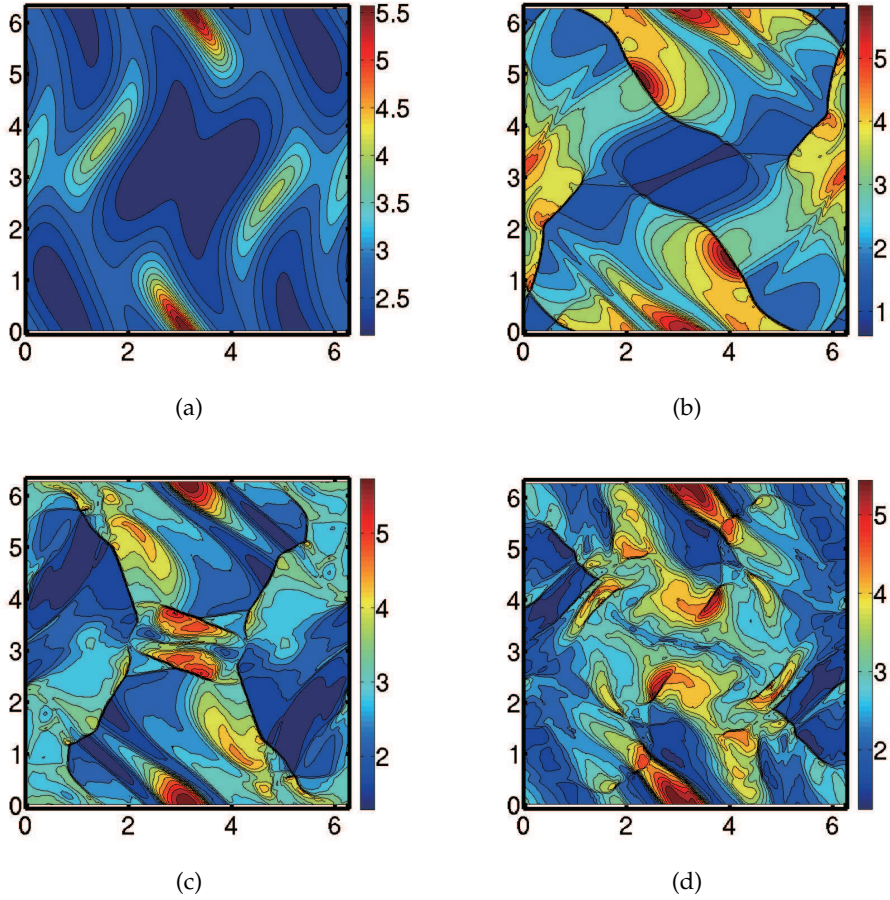


Figure 7: Contour plot of density. (a) $t=0.5$; (b) $t=2$; (c) $t=3$; (d) $t=4$. The computation was carried out with MHD_{PER} model on an $N=200$ mesh with $k=2$ scheme, $M=5$.

stage of KH and coalescence instability simulation. For large perturbations, nonlinear simulation results of KH instability, coalescence instability and Orszag-Tang vortex also clearly demonstrate the reliability of this model with non-smooth solutions. These results strongly convince us that in principle our approach is suitable for magnetically confined system. This work could be considered as a first step of our long-term MHD simulation in toroidal geometry under DG framework. The extension of the present work to 3D complex geometry is our long-term goal.

Acknowledgments

We are grateful to Dr. Weiyang Zheng, Dr. Tao Cui, and Dr. Shipeng Mao from Institute of Computational Mathematics and Scientific/Engineering Computing, and Dr.

Mengping Zhang from University of Science and Technology of China for useful discussions. The authors would also like to acknowledge the ShenMa High Performance Computing Cluster at the Institute of Plasma Physics, Chinese Academy of Sciences. This work is supported by the National Natural Science Foundation of China under Grant No. 11475219 and No. 11405208, the Science Foundation of the Institute of Plasma Physics, Chinese Academy of Sciences (DSJJ-15-JC02), and the National Magnetic Confinement Fusion Science Program of China under Grant No. 2013GB111002.

References

- [1] C. Sovinec, A. Glasser, T. Gianakon, D. Barnes, R. Nebel, S. Kruger, D. Schnack, S. Plimpton, A. Tarditi, M. Chu and the NIMROD team, Nonlinear magnetohydrodynamics simulation using high-order finite elements, *J. Comput. Phys.*, 195 (2004), 355-386.
- [2] S. Wang and Z. Ma, influence of toroidal rotation on resistive tearing modes in tokamaks, *Phys. Plasmas*, 22(2015), 122504.
- [3] W. Park, E. Belova, G. Fu, X. Tang, H. Strauss and L. Sugiyama, Plasma simulation studies using multilevel physics models, *Phys. Plasmas*, 6(1999), 1796-1803.
- [4] D. Biskamp, *Nonlinear Magnetohydrodynamics*, Cambridge University Press, Cambridge, (1993).
- [5] A. Harten, B. Engquist, S. Osher and S. Chakravarthy. Uniformly high order accurate essentially non-oscillatory schemes III. *J. Comput. Phys.*, 71(1987), 231-303.
- [6] C.-W. Shu, *Essentially Non-Oscillatory and Weighted Essentially Non-Oscillatory Schemes for Hyperbolic Conservation Laws*, NASA/CR-97-206253, ICASE Report No. 97-65, 1997.
- [7] C. Hu and C.-W. Shu, *Weighted Essentially Non-oscillatory Schemes on Triangular Meshes*, *J. Comput. Phys.*, 150(1999), 97-127.
- [8] J. Shi, C. Hu and C.-W. Shu, *A Technique of Treating Negative Weights in WENO Schemes*, *J. Comput. Phys.*, 175(2002), 108-127.
- [9] B. Cockburn and C.-W. Shu, *The Runge-Kutta local projection P^1 -discontinuous-Galerkin finite element method for scalar conservation laws*, IMA Preprint Series #388, University of Minnesota, 1988.
- [10] B. Cockburn and C.-W. Shu, *TVB Runge-Kutta local projection discontinuous Galerkin finite element method for conservation laws II: General framework*, *Math. Comput.*, 52, 186 (1989), 411-435.
- [11] B. Cockburn, S.-Y. Lin and C.-W. Shu, *TVB Runge-Kutta local projection discontinuous Galerkin finite element method for conservation laws III: One dimensional systems*, IMA Preprint Series #415, University of Minnesota, 1988.
- [12] B. Cockburn, S. Hou and C.-W. Shu, *TVB Runge-Kutta local projection discontinuous Galerkin finite element method for conservation laws IV: The multidimensional case*, IMA Preprint Series #513, University of Minnesota, 1989.
- [13] B. Cockburn and C.-W. Shu, *TVB Runge-Kutta local projection discontinuous Galerkin finite element method for conservation laws V: Multi-dimensional systems*, *J. Comput. Phys.*, 141 (1998), 199-224.
- [14] B. Cockburn and C.-W. Shu, *Runge-Kutta Discontinuous Galerkin Methods for Convection-dominated Problems*, NASA/CR-2000-210624, ICASE Report No. 2000-46.
- [15] C.-W. Shu, *A brief survey on discontinuous Galerkin methods in computational fluid dynamics*, *Adv. Mech.*, 43, 6(2013), 541C554.

- [16] A Dender, F. Kemm, D. Kröner, C.-D. Munz, T. Schnitzer and M. Wesenberg, Hyperbolic Divergence Cleaning for the MHD Equations, *J. Comput. Phys.*, 175 (2002), 645-673.
- [17] C. Altmann, An Explicit Discontinuous Galerkin Scheme with Divergence Cleaning for Magnetohydrodynamics, *Lecture notes in Computational Science and Engineering*, Vol. 76, Springer, Berlin, 357-364, 2011.
- [18] G. Töth, The $\nabla \cdot \mathbf{B} = 0$ constraint in shock-capturing magnetohydrodynamics codes, *J. Comput. Phys.*, 161 (2000), 605-652.
- [19] S. Li, High order central scheme on overlapping cells for magneto-hydrodynamic flows with and without constrained transport method, *J. Comput. Phys.*, 227 (2008), 7368-7393.
- [20] F. Li, L. Xu and S. Yakovlev, Central discontinuous Galerkin methods for ideal MHD equations with exactly divergence-free magnetic field, *J. Comput. Phys.*, 230 (2011), 4828-4847.
- [21] F. Li and L. Xu, Arbitrary order exactly divergence-free central discontinuous Galerkin methods for ideal MHD equations, *J. Comput. Phys.*, 231(2012), 2655-2675.
- [22] F. Li and C.-W. Shu, Locally Divergence-Free Discontinuous Galerkin Methods for MHD Equations, *J. Sci. Comput.*, 22 (2005), 413-442.
- [23] S. Yakovlev, L. Xu and F. Li, Locally divergence-free central discontinuous Galerkin methods for ideal MHD equations, *J. Comput. Sci-Neth.*, 4 (2013), 80-91.
- [24] B. Cockburn and C.-W. Shu, The Runge-Kutta discontinuous Galerkin method for conservation laws V: multidimensional systems, *J. Comput. Phys.*, 141 (1998), 199-224.
- [25] S. Gottlieb, C.-W. Shu and E. Tadmor, Strong stability-preserving high-order time discretization methods, *SIAM Rev.* 43 (2001), 89-112.
- [26] C.-W. Shu, Essentially non-oscillatory and weighted essentially non-oscillatory schemes for hyperbolic conservation laws, in: B. Cockburn, C. Johnson, C.-W. Shu, E. Tadmor, A. Quarteroni (Eds.), *Advanced Numerical Approximation of Nonlinear Hyperbolic Equations*, Lecture Notes in Mathematics, vol. 1697, Springer, Berlin, 325-432, 1998.
- [27] R. Keppens, G. Töth, R. Westermann and J. Goedbloed, Kelvin-Helmholtz instability with parallel and anti-parallel magnetic fields, *J. Plasma Phys.*, 61, 1(1999), 1-19.
- [28] D. Longcope and H. Strauss, The coalescence instability and the development of current sheets in two dimensional magnetohydrodynamics, *Phys. Fluids B*, 5(1993), 2858-2869.